Pergamon

*Int. J. Heat Mass Transfer.* Vol. 38, No. 2, pp. 267–274, 1995

0017-9310/95 $9.50+0.00

0017-9310(94)00143-X

# Use of a laser-induced fluorescence thermal imaging system for local jet impingement heat transfer measurement

D. J. BIZZAK and M. K. CHYU†

Department of Mechanical Engineering, Carnegie Mellon University, Pittsburgh, PA 15213-3890, U.S.A.

(*Received* 4 *August* 1993 *and in final form* 13 *May* 1994)

**Abstract**—In this paper the efficacy of a novel thermal imaging system designed for use in the study of local convective heat transfer is examined. The transient temperature measurements employed to calculate local heat transfer coefficients in this study rely on the temperature-sensitive fluorescence properties of a europium-doped lanthanum oxysulfide ($La_2O_2S:Eu^{3+}$) thermographic phosphor. A series of temperature–time data sets acquired during the heat-up of a test surface, oriented normal to an impinging heated jet, are used to calculate the local heat transfer coefficient about the stagnation point. These results are qualitatively compared to theoretical predictions and previous experimental observations to evaluate the ability to detect expected flow-field phenomena, such as the initial thinning of the boundary layer near the stagnation point and the eventual laminar to turbulent transition of boundary-layer flow away from the stagnation point. In addition, the measured stagnation point Nusselt number data are compared with theoretical and pertinent empirical data. The agreement of the stagnation point heat transfer in this comparison is excellent, with the variation between measured values based on the laser-induced fluorescence transient surface temperature measurements and existing data well within the bounds of the experimental measurement uncertainty of the present technique.

## INTRODUCTION

In this study the heat transfer characteristics of axisymmetric jet impingement on a flat surface are examined to assess the viability of using a novel laser-induced fluorescence (LIF) thermal imaging system for general heat transfer studies. This LIF system exploits the temperature sensitivity of both the fluorescence intensity and lifetime of certain europium-doped lanthanum oxysulfide ($La_2O_2S:Eu^{3+}$) emission lines. The temperature sensitive emissions that may be employed are the 512-nm triplet, active from approx. −70 to 60°C, and the 538-nm doublet, which is useful for temperature measurements in the range of 100–230°C [1]. Fluorescent images of the 512-nm triplet, along with that of the relatively temperature-insensitive 620-nm emission line, are acquired. The ratio of the integrated intensities of these two emissions, which can be accurately correlated to temperature, and intensity data from a reference isothermal surface image permits determination of temperatures at several discrete locations on the test surface.

The temperature sensitivity of the fluorescence intensity or lifetime of certain phosphors, commonly referred to as "thermographic" phosphors, has been successfully exploited for surface temperature measurement by several researchers. Goss and Smith [2] used the ratio of two emission lines of dysprosium-doped yttrium aluminum garnet ($YAG:Dy^{3+}$) crystals embedded in a thermal-setting plastic to determine local surface temperatures during the combustion of the test specimen. In addition, Lutz *et al.* [3] and Noel *et al.* [4] have used the approach based on the fluorescence lifetime sensitivity of certain rare-earth phosphors for temperature measurements on a heated turbine disk and on a first-stage stator vane in an operating turbine engine, respectively. Despite these successes in discrete-point measurement, limitations with respect to the capability for two-dimensional temperature mapping or data accuracy have prevented use of thermographic phosphor techniques for measuring heat transfer. By recording the fluorescence signal during its decay, the authors have combined the advantages of emission intensity and decay time methods in a system that is capable of accurate (±0.5°C), two-dimensional temperature measurement [5, 6].

To assess the suitability of LIF temperature measurements for the study of local convective heat transfer using a transient heat transfer technique, a problem for which both theoretical and empirical data are available for comparison is examined. Jet impingement heat transfer is such a problem, in which a plethora of data exists due to its practical significance. Jet impingement has long been an attractive means of enhancing convective heat or mass transfer over a heated, cooled or drying surface, since it is possible to produce very high local transfer rates with minimal

† Author to whom correspondence should be addressed.

## NOMENCLATURE

| | | | |
|---|---|---|---|
| $C$ | correlation constant | $z$ | axial distance between jet and impinged surface. |
| $D$ | impinged disk diameter | | |
| $d$ | jet diameter | | |
| $h$ | heat transfer coefficient | | |
| $k$ | thermal conductivity | Greek symbol | |
| $Nu$ | Nusselt number | $\alpha$ | thermal diffusivity. |
| $Pr$ | Prandtl number | | |
| $Re$ | Reynolds number | | |
| $T$ | temperature | Subscripts | |
| $t$ | time | i | initial |
| $x$ | lateral distance from center of jet (Fig. 3) | j | jet |
| | | o | stagnation point. |

fluid consumption. For the simplest configuration of an axisymmetric jet oriented normal to a surface, a sufficient database of theoretical and empirical information exists to allow assessment of the measurement capabilities of the LIF thermal imaging system. This assessment includes a qualitative evaluation to verify the ability to resolve local phenomena, as well as a quantitative examination of the results to gauge the measurement accuracy and precision of the system.

## SURFACE HEAT TRANSFER AND TEMPERATURE MEASUREMENT SYSTEM

The local heat transfer distribution over a flat surface impinged by an axisymmetric jet is determined using a transient technique. Such a transient approach has been demonstrated to be very effective for determining the local surface heat transfer coefficient with other thermographic methods, e.g. the liquid crystal technique [7, 8] and the thermal paint method [9]. The foundation of this technique is the assumption that the response of an initially isothermal test surface to a constant temperature impinging jet is similar to that of a semi-infinite solid whose surface is subjected to a step change in ambient temperature. The analytical solution of this problem yields the following expression for the front-surface temperature response:

$$\frac{T(t)-T_i}{T_j-T_i} = 1-\exp\left(\frac{h^2\alpha t}{k^2}\right)\operatorname{erfc}\left(\frac{h\sqrt{(\alpha t)}}{k}\right) \quad (1)$$

where $T(t)$ is the local surface temperature as a function of time, $T_j$ is the jet temperature, $T_i$ is the initial surface temperature, $t$ is the time for the local surface temperature to reach $T(t)$ and $h$ is the local convective heat transfer coefficient. The remaining parameters—$\alpha$ and $k$—are the thermal diffusivity and thermal conductivity, respectively, of the solid. This equation is solved for several temperature–time data sets to obtain an average local heat transfer coefficient at 58 discrete surface locations.

The fundamental assumption that the test surface behaves as a semi-infinite solid is valid provided that the duration of the transient is sufficiently short to avoid heat penetration to the back surface of the test specimen. With local heating due to jet impingement, heat transfer is no longer one-dimensional, and lateral conduction within the test surface will begin to affect front surface temperature response. Since use of multiple temperature data sets is desirable to minimize the uncertainty of the calculated heat transfer coefficients, it is necessary to establish the time at which heating of the back surface will begin to affect the results. For the expected impingement heat transfer rates in this study, the results of a finite-difference computer modeling suggest the adverse effects of back-surface heat penetration may be avoided if the transient is limited to 30 s.

Surface temperatures during the transient are nonintrusively measured using the LIF thermal imaging system shown schematically in Fig. 1. The key elements of the system include: (1) the laser excitation hardware; (2) the phosphor temperature sensor; (3) the image-collection optics; and (4) the imaging subsystem. Each of these components or subsystems are briefly discussed below.

Ultraviolet (u.v.) excitation of the phosphor coating of the test surface is provided by the tripled output (355 nm) of an Nd:YAG pulsed laser. The tripled

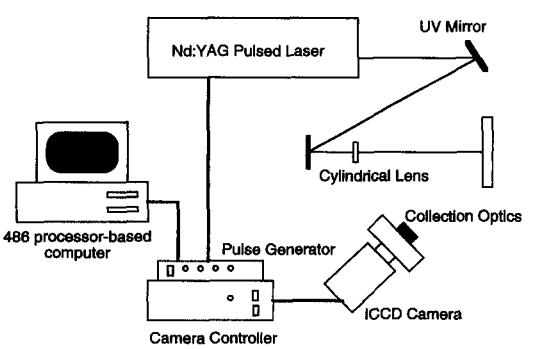


Fig. 1. LIF thermal imaging system.

output from the laser is generated by passing the 1064-nm primary output through a harmonic generator to obtain a beam of 355-nm wavelength light, along with residual components of the primary and first harmonic (532 nm). These undesired portions of the laser beam are then effectively separated and eliminated by a beam splitter assembly. The energy of the 355-nm output beam from the splitter, which is delivered over a 5–6 ns pulse, is approx. 75 mJ.

The critical element of the LIF thermal imaging system is the thin layer of europium-doped lanthanum oxysulfide ($La_2O_2S:Eu^{3+}$) phosphor that is applied to the test surface. When subjected to u.v. excitation, this phosphor fluoresces brightly in the visible spectrum. The emission spectrum of this phosphor, as for other rare-earth doped phosphors, comprises numerous sharp emission lines. Certain of these lines exhibit a temperature sensitivity that is manifested in changes to both the fluorescence intensity and decay time. For $La_2O_2S:Eu^{3+}$ the steady-state intensity of the 512-nm emission triplet decreases by a factor of 2.5 as temperature is increased from 20 to 60°C, while the lifetime over this temperature range decreases by an order of magnitude. Collection of the fluorescence signal during its decay permits a precise determination of temperature based on both of these sensitivities. However, since the initial fluorescence amplitude at a given surface location is dependent on both the excitation energy and phosphor coating density, use of the 512-nm fluorescence signal alone will not permit accurate two-dimensional thermometry. To compensate for these spatial variations in the signal, the intensity of the 512-nm emission triplet is ratioed to that of the 620-nm emission. The intensity of the latter emission, which is relatively immune to temperature, provides a reference signal whose intensity variation due to spatial nonuniformity in excitation energy or phosphor density is identical to that of the 512-nm emission. As a result, this intensity ratio can be accurately correlated to temperature regardless of the absolute magnitude of the local temperature-sensitive emission.

The signals from the two emission lines used for temperature measurement are gathered using the optical setup shown in Fig. 2. The fluorescent image of the test surface following excitation is collected by a 150 mm enlarger lens and split into equal length optical paths that are focused side-by-side onto a CCD image detector. One optical path passes through a 510-nm narrow bandpass filter, while the other is directed through a 620-nm bandpass and a neutral density filter. The neutral density filter is required to reduce the intensity of the 620-nm fluorescence signal to a level comparable to that of the 510-nm signal, because the intensity and lifetime of the 620-nm emission is considerably greater than that of the temperature sensitive 510-nm emission.

The major components of the imaging subsystem are an image-intensified CCD detector, a gate pulse generator, a detector controller and a microcomputer for overall system control. Concurrent with laser excitation, the detector simultaneously records images of the surface at the emission-line wavelengths of interest. The timing and duration of image acquisition are controlled by the gate pulse generator, which issues a square-wave pulse that enables the image intensifier. The duration of this pulse defines the fluorescence signal integration period. In this study, the pulse generator is set to issue a 40-$\mu$s pulse approx. 280 ns in advance of laser firing. To prevent exposure of the detector during read-out following image capture, the controller disables the pulse generator until image data have been read and stored to disk. Finally, a 80486 processor-based computer provides overall sys-

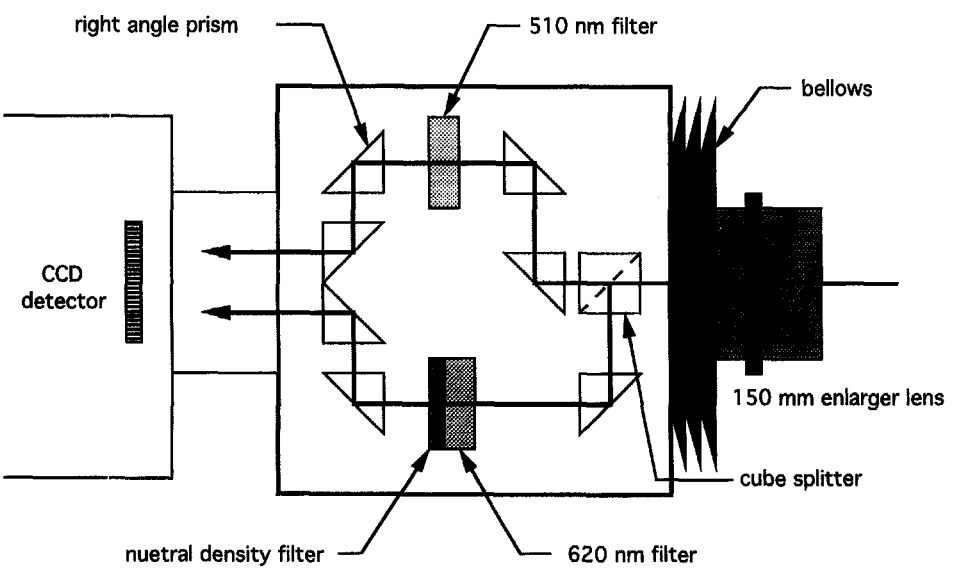


Fig. 2. LIF image collection optics.

tem control and is used in image post-processing to calculate emission intensity ratio values that are then used in conjunction with the phosphor calibration to determine local surface temperatures.

## EXPERIMENTAL SETUP AND PROCEDURE

The apparatus for the heated jet impingement tests is shown schematically in Fig. 3. One surface of the 6.4 by 127 mm diameter quartz disk that serves as the test specimen is coated with a 25-$\mu$m layer of $La_2O_2S:Eu^{3+}$. The phosphor layer is prepared by the settling technique similar to the method to coat a cathode-ray tube or a television screen. Since the 25-$\mu$m phosphor coating accounts for less than 0.1% of the thermal resistance normal to the disk, the material properties of clear-fused quartz, which are assumed to be representative of those of the entire phosphor-coated disk, are used in the calculation of local heat transfer coefficients, based on equation (1).

The 5.3-mm diameter jet is located along a radius with the center of the jet approx. $0.25D$ from the disk origin. This positioning ensures that radial flow outward from the stagnation point in the measurement area will not be affected by the presence of the disk shaft. A plastic stop around the circumference of the stainless steel tube from which the heated jet issues ensures repeatable positioning of the jet at a dimensionless axial distance from the disk surface of $z/d = 2$. As illustrated in the figure, a 6 by 65-mm region perpendicular to the horizontal disk radius is illuminated by the laser.

Prior to conducting a test, the jet is removed from its mounting bracket and preheated. The desired volumetric flow rate to the jet is set using a low-flow, precision rotameter. Metered flow exiting the rotameter is heated in a downstream section of heat-traced copper piping. The jet outlet air temperature is measured using a thermocouple and is controlled by varying the power supplied to the constant flux coil heater element wrapped around the 600-mm section of 9.5-mm inside-diameter copper piping. For the jet impingement tests described here a steady-state jet outlet temperature in the range of 50–55°C is reached within 15 min.

When a stable jet temperature is reached, the laser is activated to acquire a reference isothermal surface image. The ambient air temperature at the time this image is collected is recorded for later use in data post-processing. After the reference image has been stored, 15 frames of fluorescent images are collected. Each image frame represents the integrated fluorescence signal accumulated over 12 laser pulses, or 1.1 s, with the signal integration period following each pulse being 40 $\mu$s. Heated impingement flow from the jet is promptly initiated after the first image frame is collected, and the time between collection of the first image and the start of heated jet flow is clocked using a stop watch. The jet can typically be manually positioned in its mount within 5 s after image collection is commenced.

Following acquisition of the raw fluorescent image data, the laser is placed in the standby mode (i.e. the flash lamp is deactivated), and the data are processed. Local Nusselt numbers for 58 locations on the disk surface, equally-spaced at intervals of 0.8 mm, are calculated. For each surface location, intensity data from a $5 \times 8$ pixel array, which for the 1-m viewing distance employed in this study corresponds to a test surface area of 0.8 by 1.3 mm, are used to calculate local surface emission-line intensity ratios. These intensity ratios are then divided by the value of the intensity ratio at the same surface location obtained from the isothermal reference image. These "corrected" intensity ratios may be converted to temperatures using a phosphor calibration curve. To permit direct determination of temperature, however, the generic phosphor calibration data must be normalized by value of the emission intensity ratio at the reference temperature. The temperature–time data sets for each image frame that is collected during the initial 30 s of heated jet flow then serve as input to a software rou-

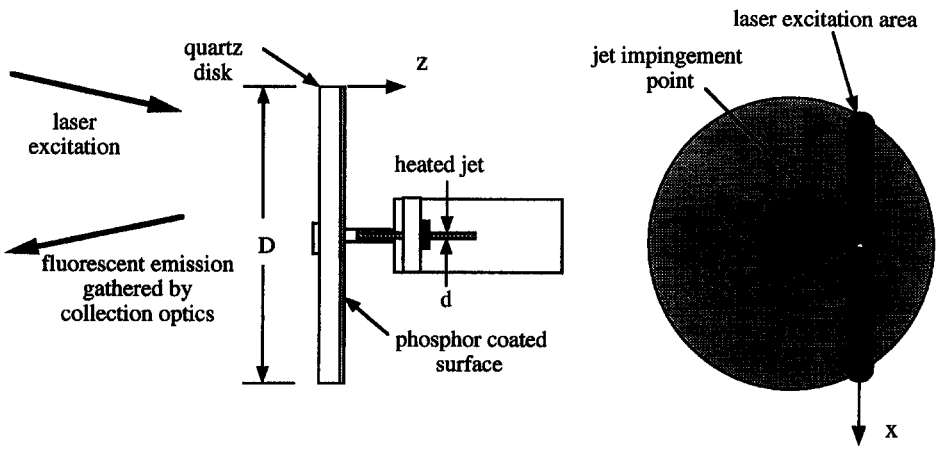


Fig. 3. Jet impingement experimental setup.

tine that implicitly solves equation (1) for the local heat transfer coefficient.

For each fluorescent image acquired after the initiation of jet flow, but before 30 s have elapsed, equation (1) is solved for each of the 58 discrete surface locations. The calculated heat transfer coefficient at each location is then averaged over the number of image frames collected during the transient (nine frames are generally acquired during the 30-s transient). These frame-averaged heat transfer coefficients are then used along with the thermal conductivity of the air at the film temperature, $(T_j + T_i)/2$, to calculate local Nusselt numbers. For typical ambient and jet air temperatures, use of the film temperature for determination of the thermal conductivity of air yields Nusselt numbers that will deviate by no more than 6% from those that would be calculated using the thermal conductivity based on the local near-surface air temperature.

## RESULTS AND DISCUSSION

In this section results of the heated jet impingement experiment are presented and discussed. The first focus of discussion is the local Nusselt number profile data, which provide insight into the transport characteristics of the jet impingement. To quantitatively evaluate the quality of the results obtained using the LIF thermal imaging technique for transient surface temperature measurement, stagnation point heat transfer data are also presented and compared with available theoretical and empirical data. Finally, the uncertainty of the reported results, as well as the repeatability, are briefly discussed.

### *Local heat transfer profiles*

Local Nusselt number data for four different jet Reynolds numbers ($Re_j$) are presented in Fig. 4. In the figure, the local Nusselt number is plotted as a function of the dimensionless distance from the stagnation point. The axial separation between the jet and impingement surface in these tests is $z/d = 2$.

Qualitatively, the Nusselt number profiles exhibit distinctive features consistent with analytical predictions of the flow field in the impingement and wall jet-flow regimes. Heat transfer may be observed to increase away from the stagnation point, reaching a maximum at $x/d = 0.5$. This local variation is attributable to the acceleration of radial flow from the stagnation point, which causes the radial velocity to increase as the boundary layer thins. The location of the local maximum is consistent with results of Kezios' analytical evaluation of axisymmetric jet impingement flow in which the boundary layer was found to reach a minimum thickness in an annular region centered about $x/d = 0.5$ [10]. The other interesting feature of the heat transfer profiles for the two highest jet Reynolds numbers is the appearance of secondary heat transfer peaks in the region $x/d = \pm 1.7$–$2.0$.

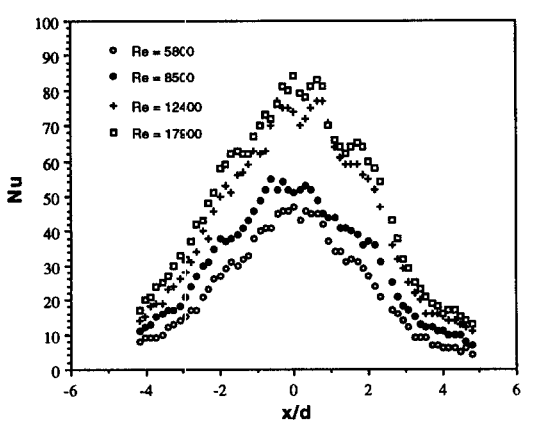


Fig. 4. Jet impingement local Nusselt number profiles.

Gardon and Akfirat [11] argued that these secondary peaks correspond to the location at which wall jet boundary-layer flow makes the transition from laminar to turbulent flow. They observed such secondary heat transfer peaks in their evaluation of the local convective heat transfer produced by both slot and axisymmetric jets. For axisymmetric jets with a jet-to-surface separation of $x/d = 2$, they noted the occurrence of this peak for $Re_j = 1.4 \times 10^4$ at $x/d = \pm 1.8$. As the jet Reynolds number was increased, the location of this secondary peak moved outward from the stagnation point, reaching $x/d = \pm 2.0$ at $Re_j = 2.0 \times 10^4$.

The profiles in Fig. 4 are generally consistent with these observations. First, the range of the location of the peaks in the present study ($x/d = \pm 1.7$–$2.0$) is similar to that noted by Gardon and Akfirat. It is appropriate to note, however, that an exact correspondence between these studies would not be expected because the boundary-layer flow transition from laminar to turbulent flow is dependent on the design of the jet nozzle (i.e. the exit design affects the rate of jet spread) and the initial jet turbulence level. Another distinguishing feature of the laminar-to-turbulent flow transition location noted in both studies is its dependence on the jet Reynolds number. That is, irrespective of the exact distance from the stagnation point at which the boundary-layer flow becomes turbulent for a given jet Reynolds number, this distance increases with the Reynolds number. This behavior can be observed in the Nusselt number profiles for the two highest jet Reynolds numbers, in which the location of the secondary peaks for $Re_j = 1.79 \times 10^4$ occur slightly outboard of the ones for $Re_j = 1.24 \times 10^4$.

### *Stagnation point heat transfer*

Most theoretical and experimental investigations of jet impingement heat transfer have focused on the value of the stagnation point heat transfer. Near the stagnation region in which laminar flow prevails, solution of the Navier–Stokes and energy equations yields a relation for the stagnation point Nusselt number of the following form:

$$Nu_o = C\,Re_j^{0.5}\,Pr^{0.4} \quad (2)$$

where $Nu_o$ is the Nusselt number based on the jet nozzle diameter, $Re_j$ is the jet Reynolds number based on the diameter of the jet, $Pr$ is the Prandtl number and $C$ is a constant dependent on the local radial velocity gradient, which, in turn, is dependent on the geometry of the impingement surface (e.g. a sphere or flat plate) and the structure of the impinging jet.

A turbulent jet develops from the nearly uniform velocity flow emerging from a nozzle or orifice. Downstream of its origin, the structure of the jet consists of a uniform velocity potential core surrounded by a mixing region formed by the entrainment of ambient fluid along the free boundary layer of the jet. The inner boundary of the mixing region moves radially inward so that, at a downstream distance of approx. 4–7.5 times the initial jet diameter, the potential core no longer exists. For impingement flow on a flat plate at jet-to-surface axial spacing in which the potential core remains intact, evaluation of the constant $C$ in equation (2) yields a value of 0.535, according to Nakatogawa *et al.* [12].

Numerous experimental investigations of jet impingement heat transfer have also been conducted in which the influence of parameters such as the jet diameter, jet Reynolds number, jet-to-surface axial spacing, turbulence level, etc. on the stagnation point heat transfer have been investigated. Due to the abundance of such studies, it is necessary to restrict discussion to those deemed relevant to the present jet impingement test results. The primary criteria used to evaluate the relevance of previous studies are the jet Reynolds number, jet diameter and jet-to-surface axial spacing. Results of pertinent jet impingement heat transfer studies are briefly discussed below.

Smirnov *et al.* [13] examined stagnation region jet impingement heat transfer using submerged water jets with diameters from 2.5 to 36.6 mm. The Reynolds number in these tests was varied from 50 to $3.1 \times 10^4$, and the dimensionless spacing between the jet nozzle and the impingement plate was $0.5 \leqslant z/d \leqslant 10$. In these experiments an impinging water jet cooled a 48-mm diameter heated copper calorimeter plate. The temperature of the calorimeter was held constant by a circulating water bath. The input heat flux to the surface, as determined by the measurements of the steady-flow, circulating bath inlet and outlet temperatures, in conjunction with the fluid properties based on the conditions at the throat of the jet, was used to calculate the stagnation point Nusselt number. Results for axial jet-to-surface spacing in the range $0.5 \leqslant z/d \leqslant 10$ were correlated by the following relation:

$$Nu_o = 0.034 d^{0.9}\,Re_j^{0.64}\,Pr^{0.33}\exp(-0.037 z/d) \quad (3)$$

where $d$ is the diameter of the jet nozzle in mm. These results were found to be in general agreement with previous empirical data for air and water jets in the axial spacing and Reynolds number range of interest, and the correlation was reported to be valid for $1.6 \times 10^3 \leqslant Re_j \leqslant 5.0 \times 10^4$ and $0.7 \leqslant Pr \leqslant 10$.

The lateral variation of the heat transfer coefficient for two-dimensional slot and axisymmetric jets within and beyond the stagnation region was examined by Gardon and Akfirat [11]. For the axisymmetric jet, local heat transfer coefficient profiles for jet Reynolds numbers from $2.5 \times 10^3$ to $2.8 \times 10^4$ were determined by measuring local surface heat fluxes using miniature surface-mounted flux gauges. The diameter of the jet nozzle in these tests was 6.4 mm, and the jet-to-surface spacing was $z/d = 2$. To permit comparison with the present results, values of the stagnation point Nusselt number were calculated from the reported local stagnation point heat transfer coefficients.

The stagnation point Nusselt numbers from the present study are compared with the heat transfer correlations discussed above and Gardon and Akfirat's data in Fig. 5. In the figure the current stagnation Nusselt number results are consistently higher than those measured by Smirnov *et al.* [13]. The use of the Smirnov *et al.* correlation, however, may be inappropriate for predicting stagnation point heat transfer for small diameter jets such as the one employed in this study, since their Nusselt numbers are based on the measured heat transfer to a 48-mm diameter calorimeter. Local surface heat transfer, as illustrated in Fig. 4, falls off rapidly with distance from the stagnation point, so it is likely that their measurements for small diameter jets significantly underestimate the actual stagnation point heat transfer. As may be seen in Fig. 5, much better agreement is seen when the present results are compared to both the analytical prediction and Gardon and Akfirat's data. For data across the range $2.5 \times 10^3 \leqslant Re_j \leqslant 3.2 \times 10^4$ from the present study, the stagnation point Nusselt number can be related to the jet Reynolds number by the correlation below,

$$Nu_o = 3.8 + 0.56 Re_j^{0.5}. \quad (4)$$

The correctness of this fit to the acquired data is illustrated in Fig. 6.

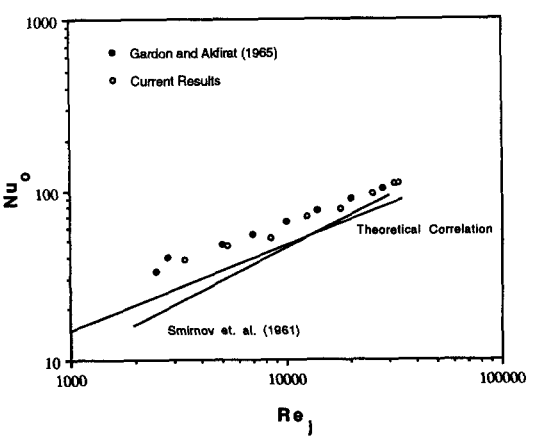


Fig. 5. Stagnation point Nusselt number comparison.

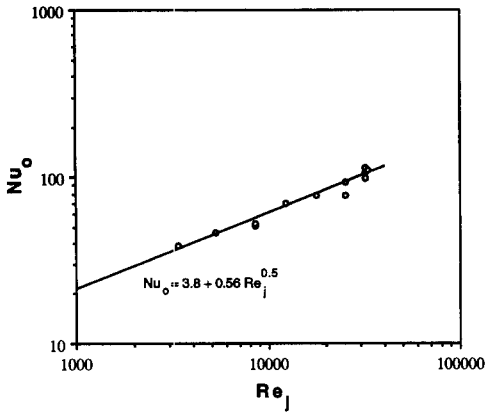


Fig. 6. Present stagnation point Nusselt number correlation.

*Measurement uncertainty and repeatability*

Based on the single-sample principle by Kline and McClintock [14], the uncertainty in the reported local Nusselt numbers in this study is estimated to be 11%. This estimate encompasses the uncertainty in the calculation of the heat transfer coefficient due to initial surface and jet air temperature measurement error, the error in timing the initiation of heated jet impingement and LIF system surface temperature measurement error. In addition, the estimate includes the 6% uncertainty in the Nusselt number, due to the use of the film temperature, rather than local surface temperature, in the determination of the thermal conductivity of air. Consequently, the approx. 5% deviation between the measured stagnation point Nusselt numbers and the theoretical values from equation (2) is within the uncertainty band of the measurements.

To ascertain the test-to-test variation in the calculated local Nusselt numbers due solely to surface temperature measurement error, three independent jet impingement tests for $Re_j = 8.5 \times 10^3$ were conducted, and the Nusselt number profiles from these tests are displayed in Fig. 7. The average deviation of the local Nusselt numbers from the averaged value for all three tests is 5%, and the maximum deviation at any surface location is 19%. The maximum deviation, however, occurs at a distant location from the stagnation point, where the value of the Nusselt number is only 10, so this deviation represents an error of only $\pm 2$ in the Nusselt number.

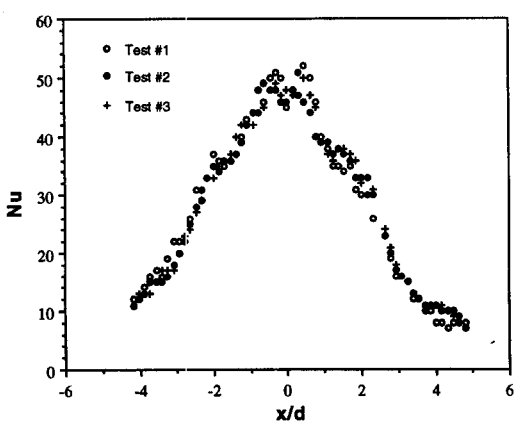


Fig. 7. Local heat transfer measurement repeatability.

## CONCLUSIONS

Through the examination of the local heat transfer from an impinging axisymmetric jet, this study has demonstrated the efficacy of the non-intrusive LIF thermal imaging technique for transient two-dimensional surface temperature measurement, suitable for use in calculating local heat transfer rates. The reported local heat transfer profiles near the stagnation region are of sufficient accuracy to detect qualitative features of the near-surface flow field predicted by theoretical analyses and previously observed by researchers using conventional heat transfer measurement techniques. Furthermore, measured values of the stagnation point heat transfer from this study agree to within 5% of theoretical prediction and previous empirical data from a similar experiment. This deviation is well within the estimated Nusselt number uncertainty of $\pm 11\%$, which is comparable with the uncertainty obtained using conventional and more modern optical temperature measurement techniques. Based on these results and its inherent advantages over other temperature measurement methods, namely non-intrusive measurement and high spatial resolution capabilities, LIF thermal imaging promises to be a powerful new optical technique, suitable for use in the study of local convective heat transfer.

*Acknowledgements*—This work, in part, has been supported by the NASA Marshall Space Flight Center, the IBM Corporation, and an NSF research equipment grant (CTS-9112284).

## REFERENCES

1. W. H. Fonger and C. W. Struck, $Eu^{+3}$ $^5D$ resonance quenching to the charge-transfer states in $Y_2O_2S$, $La_2O_2S$, and LaOCl, *J. Chem. Phys.* **52,** 6364–6372 (1970).
2. L. P. Goss and A. A. Smith, Surface thermometry by laser-induced fluorescence, *Rev. Sci. Instrum.* **60,** 3702–3706 (1989).
3. S. S. Lutz, W. D. Turley, H. M. Borella, B. W. Noel, M. R. Cates and M. R. Probert, Remote temperature measurement instrumentation for a heated rotating turbine disk, Los Alamos National Laboratory Technical Report, LA-UR-88-599 (1988).
4. B. W. Noel, H. M. Borella, W. Lewis, W. D. Turley, D. L. Beshears, G. J. Capps, M. R. Cates, J. D. Muhs and K. W. Tobin, Evaluating thermographic phosphors in an operating turbine engine, ASME paper 90-GT-266 (1990).
5. M. K. Chyu and D. J. Bizzak, Surface temperature measurement using a laser-induced fluorescence thermal imaging system, *J. Heat Transfer* **116,** 263–266 (1994).
6. D. J. Bizzak, A laser-induced fluorescence thermal imaging system for the study of local convective heat transfer, Ph.D. Thesis, Carnegie Mellon University, Pittsburgh, PA (1993).

7. D. E. Metzger and D. E. Larson, Use of melting point surface coating for local convection heat transfer measurements in rectangular channel flows with 90-deg. turns, *J. Heat Transfer* **108,** 48–54 (1986).
8. Z. Wang, P. T. Ireland and T. V. Jones, An advanced method for processing liquid crystal video signals from transient heat transfer experiments, ASME Paper 93-GT-282 (1993).
9. D. E. Metzger, R. S. Bunker and G. Bosch, Transient liquid crystal measurement of local heat transfer on a rotating disk with jet impingement, *J. Turbomach.* **113,** 52–59 (1991).
10. S. P. Kezios, Heat transfer in the flow of a cylindrical jet normal to an infinite plate, Ph.D. Thesis, Illinois Institute of Technology, Chicago, IL (1956).
11. R. Gardon and J. C. Akfirat, The role of turbulence in determining the heat-transfer characteristics of impinging jets, *Int. J. Heat Mass Transfer* **28,** 977–985 (1965).
12. T. Nakatogawa, N. Nishiwaki, M. Hirata and K. Torii, Heat transfer of round turbulent jet impinging normally on flat plate, *Proceedings of the Fourth International Heat Transfer Conference*, Vol. 2, FC 5.2 (1970).
13. V. A. Smirnov, G. E. Verevochkin and P. M. Brdlick, Heat transfer between a jet and a held plate normal to flow, *Int. J. Heat Mass Transfer* **2,** 1–7 (1961).
14. S. J. Kline and F. A. McClintock, Describing uncertainties in single sample experiments, *Mech. Engng* **75,** 3–8 (1953).